# In situ X-ray Photoelectron Spectroscopy of Electrochemically Active Solid-Gas and Solid-Liquid Interfaces

Axel Knop-Gericke[1,*], Verena Pfeifer[1,2], Juan-Jesus Velasco-Velez[3], Travis Jones[1], Rosa Arrigo[4], Michael Hävecker[3], R. Schlögl[1,3]

1: Fritz-Haber-Institut der Max-Planck-Gesellschaft, Department of Inorganic Chemistry, Faradayweg 4-6, 14195 Berlin, Germany

2: Helmholtz-Zentrum Berlin für Materialien und Energie GmbH, Catalysis for Energy, Group EM-GKAT, Elektronenspeicherring BESSYII, Albert-Einstein-Str. 15, 12489 Berlin, Germany

3: Max-Planck-Institut für Chemische Energiekonversion, Deptartment of Heterogeneous Reactions, Stiftstr. 34-36, 45470 Mülheim

4: Diamond Light Source Ltd., Harwell Science & Innovation Campus, Didcot, Oxdordshire OX 11 0DE, UK

*Corresponding author: knop@fhi-berlin.mpg.de

## Abstract

In this article the application of synchrotron radiation based X-ray photoelectron spectroscopy (XPS) to the investigation of electrochemical active gas-solid and liquid-solid interfaces will be discussed. The potential of Near Ambient Pressure XPS (NAP-XPS) for the estimation of the electronic structure of electrochemically active interfaces will be described by two examples. Thereto the oxygen evolution reaction (OER) over Pt and $IrO_x$ anodes will be introduced. In particular the analysis of XP spectra measured of the Ir anode requires the development of an appropriate fit model. Furthermore the design of a reaction cells based on proton exchange membrames (PEM) and on electron transparent graphene membranes, which enables the investigation of liquid-gas and liquid-solid interfaces under electrochemical relevant conditions will be exhibited. In the last part of this article a perspective to the EMIL project at the synchrotron radiation facility BESSY will be exposed. The purpose of this project is the implementation of two new beamlines enabling X-ray photoelectron

spectroscopy in the X-ray regime from 50 eV – 8 KeV under reaction conditions. The extension to the tender X-ray regime will allow the release of higher kinetic energy photoelectrons which have a higher inelastic mean free path and therefore will enable the investigation of solid-liquid interfaces under electrochemical reaction conditions.

## 1. Introduction

The integration of renewable energies into the energy supply of many countries generates the demand of energy storage capabilities since renewable energies like solar and wind energy are characterized by intermittent supply[1]. A promising approach to store energy supplied by photovoltaic systems or wind wheels, is presented by the conversion of electricity into chemical energy realized in electrolyzers, which split water into oxygen and hydrogen[2],[3],[4]. The hydrogen will be bonded by a subsequent catalytic reaction into methanol or ammonia. Nowadays noble metals based electrodes are used as anodes in electrolyzers. Since they are rare and very expensive the application of noble metal based electrolyzers on large scale will fail. Therefore other electrode materials to perform water splitting are requested. The search for alternative materials will be probably more successful, if the processes taking place at the interface between the noble metal electrode and water are understood on a molecular level. These processes can be studied for a short time by in situ methods like photoelectron spectroscopy. In this short review the development of electrochemical cells, which enable the electron spectroscopic access to electrochemically active gas-solid and liquid-solid interfaces will be described. The electronic structure of an electrochemically active vapor-solid interface can be investigated by means of a proton exchange membrane (PEM). The cell dedicated to the investigation of solid-gas interfaces consists of a polymer, which is proton conducting, when it is hydrated. The liquid water diffuses through the membrane and reaches as water vapor the working electrode deposited on the surface of the membrane. A second type of electrochemical cell based on the application of graphene membrane, which were

passed by the photoelectrons released by the X-ray excitation. Two examples of X-ray spectroscopy studies of vapor-solid interfaces in the oxygen evolution reaction over Pt and Ir based anodes and the electroplating of graphene by Co will be discussed as an example of the study of an electrochemically active liquid-solid interface. The in (N)AP-XPS studies present here, were performed by the use of synchrotron radiation. The concept of in situ photoelectron spectroscopic measurements through a graphene membrane will be compared to the alternative dip and drop an approach.

## 2. PEM cell

The first approach enabling measurements of surface sensitive X-ray photoelectron spectra (XPS) [1]arrigo under electrochemical relevant conditions was realized by the application of a PEM (proton exchange membrane). A schematic drawing of this cell is shown in Figure 1. In this approach a Nafion membrane covered by the working electrode which was sputtered on one side of the Nafion membrane was used, whereas the counter electrode (Pt) was sputtered on the back side. The thickness of the electrodes was estimated in the order of 70 nm. The electrodes are characterized by random cracks which are due to desiccation enabling the water to diffuse through the counter electrode and the Nafion to the working electrode. The water enables not only the ion conductivity of the Nafion membrane due to the hydration, but it supplies as well the reaction molecules to the working electrode due to the permeability of the membrane and the cracks in the electrode layers. One drawback of the first design is given by the limited capacity of the water reservoir. The water container has to be refilled after 50 min of measurements, which requires a transfer of the sample and therefore an interruption of the experiments. Thus the second version of the cell avoids this disadvantage by the implementation of a dynamic water supply. In addition the second cell is equipped by a reference electrode as shown in Figure 1. Due to the low pressure of 0.2 mbar at the vacuum side of the membrane the water will be present at the low pressure side mainly

as water vapor. The recipient hosting the PEM cell is equipped by a mass spectrometer which enables the detection of evolved oxygen or hydrogen.

### 3. Oxygen evolution reaction using a Pt anode

The oxygen evolution reaction (OER) over Pt was studied by Arrigo et al. using Nafion based electrochemical cells[5] . The sputtered electrodes were formed by interconnected nanoparticles with a thickness of about 70 nm onto the Nafion. XPS survey scans show beside Pt and O also the presence of C and F indicating the porous structure of the Pt electrode necessary for mass transport (not shown), since these signals are related to the Nafion membrane. The deconvoluted Pt4f core level spectra of the Pt anode are characterized by three components (Fig.2). The main contribution assigned to metallic Pt is characterized by a binding energy of 71 eV attended by two further peak profiles at 71.6 eV and 72.5 eV. The component with a binding energy of 72.5 eV and a further species with a binding energy of 74.5 eV were observed on electrochemically oxidized Pt foil in acidic media. These two features are related to Pt species with the formal valence of +2 and +4 [6,7,8] .The component at 71.6 eV is assigned to O on Pt surfaces as two dimensional surface oxide by Zhu recently [3]

Arrigo has shown, that an increase of the potential applied to the working electrode from 2V to 2.5V results in an increase in particular of the component at 71.6 eV. At the same time the mass spectrometer indicates a significantly increased amount of oxygen in the recipient hosting the working electrode. Since the abundance of the $Pt^{2+}$ increased as well when a positive voltage is applied to the working electrode, the Pt anode was exposed to ozone to enable to oxidation of the Pt anode. Figure 3 demonstrates that the treatment in ozone results in the formation of Pt2+ and even Pt4+, but no species with a binding energy of 71.6 eV is formed. The oxygen evolution reaction performed at 2V did show only a very small current.

An increase of the anode voltage to about 4V results in a reduction of the $PtO_2$ indicated by the disappearance of the $Pt^{4+}$ species and a strong decrease of the abundance of the $Pt^{2+}$ species. At the same time the Pt species characterized by a binding energy of 71.6 eV reappears and a strong activity of the OER, measured by the current, was observed. These experiments clearly show, that the Pt oxides are detrimental for the OER in water vapor. The measurements indicate a possible explanation of the of the initial Pt oxidation at RT under electrochemical control[9],[10],[11]. The electronic structure of the Pt bulk is partly decoupled from the Pt surface due to the formation of the surface oxide. This results to the reduction of the density of states in the valence band indicated by the shift of the Pt4f state by 0.6 eV (Fig. 3a). The formation of the surface oxide seems to be a prerequisite for the dissociative adsorption of water.

**4. The electronic structure of iridium and its oxides**

Iridium oxide is an often used material for anodes in electrolyzer. In order to study Ir based electrodes under conditions of the oxygen evolution reaction, a reliable curve fitting procedure has to be developed for Iridium oxide 4f core level spectra. It is well known, that Iridium metal 4f core level can be fitted by a Doniach-Šunjić line profile whereas this approach fails for Iridium oxide [12],[13]. Recent DFT calculations have shown, that the partial density of d states (PDOS(d)) in the presence of a 4f core hole is characterized by a sharp peak located 1 eV above the Fermi energy, which causes shake-up resonances at 1 eV higher binding energy compared to the main line of the Ir 4f core level spectrum [14] (see Fi4a). A second satellite structure, which has to be considered in the Ir 4f spectra 3 eV above the main line is due to the excitation of Ir d electrons, which shows a peak at about 2eV below $E_F$ to the already mentioned unoccupied states 1 eV above $E_F$ [7]. Considering the $Ir^{IV}$ main line by a Doniach-Šunjić line profile and the two satellites by Gaussian lines it is possible the get a satisfying fit of the measured Ir4f spectrum of rutile-type $IrO_2$ (Fig.4b). The Ir4f spectrum of

amorphous $IrO_x$ looks a bit more complicated since $Ir^{III}$ states and their satellite structures have to be considered additionally, in which the amorphous structure is described as an $IrO_2$ rutile structure with Ir defects (fig. 4b). Besides DFT calculations indicated that the binding energy of $Ir^{III}$ is higher that the binding energy of $Ir^{IV}$. An Ir vacancy leads to the formation of formally $O^{I-}$ species and the two additional electrons reduce two neighboring from $Ir^{IV}$ to $Ir^{III}$ [7] as shown in Fig.5.

The O K-edge X-ray absorption spectra of $IrO_2$ and the $IrO_x$ show significant differences in the pre-edge region. It is obvious, that the amorphous sample reveals a feature at 529 eV whereas the $IrO_2$ rutile-type exhibits a strong pre-edge peak at 530 eV [15] (see Fig.6). Both O K-edge spectra were calculated and it was assumed that the rutile-type $IrO_2$ contains just $O^{II-}$ species whereas the amorphous $IrO_x$ is expected to consist of a mixture of $O^{I-}$ and $O^{II-}$. A comparison of the calculated spectra shows a nice agreement with the measured data as shown in Fig.6.

The reactivity of the weakly bond $O^{I-}$ species characterized by O2p holes was tested in the stoichiometric CO oxidation at room temperature. It was clearly seen that rutile-type $IrO_2$ does not show any activity, whereas amorphous $IrO_x$ revealed a strong $CO_2$ formation rate which is decreasing as a function of time on stream, since no oxygen additional was provided [16]. O K-edge spectra measured before and after the CO exposure at 25 Pa, 2mL $min^{-1}$ CO at 298 K indicate strong differences in the pre-edge region. The intensity of the O K-edge spectrum is reduced in the entire energy range from 525-560 eV after CO exposure, but in particular in the pre-edge region around 529 eV a strong intensity drop was observed after the CO exposure. The difference spectrum (before CO exposure - after CO exposure) indicates a strong similarity to the calculated spectrum of the $O^{I-}$ species. Besides microcalorimetry measurements confirms the assumption that CO is reacting with the $O^{I-}$ species, since the

measured differential heats of reactions agree with the calculated ones for the reaction of CO with $O^{I-}$ on (113) and (110) single crystal surfaces.

The catalytic cycle is just closed if the $O^{I-}$state can be replenished again. For that purpose the amorphous $IrO_x$ sample was exposed to ozone after the CO exposure [9]. The intensity loss of the O K-edge spectrum was regained after the ozone exposure. In particular the loss at 529 eV has recovered and the difference spectrum (after ozone dosing- before ozone dosing) is similar to the calculated $O^{I-}$ spectrum. It is worth to note, that the replenished structure is not stable for a long time. Therefore it is assumed the OH-groups are required to stabilize the $O^{I-}$ sites and a treatment in a mixture of ozone and water vapor will result in a more stable surface.

These studies have demonstrated the electrophilic character of the $O^{I-}$ species, which can even oxidize CO to $CO_2$. Since these are all ex situ measurements the relevance of the observed species has to be proven by in situ measurements.

Only an in situ measurement enables the study of electronic-structure – function relationship. Therefore O K-edge XAS of an $IrO_x$ electrode deposited on a PEM were measured [17] (see Fig.7). The voltage applied to the $IrO_x$ anode was varied and O K-NEXAFS scans were recorded. It is very obvious, that there are changes in the pre edge structure as a function of the applied voltage. Figure 7d shows, that the higher the voltage the higher is the abundance of $O^{I-}$ at the surface. The evolved oxygen was measured simultaneously by a mass spectrometer. Finally there is a correlation between the $O^{I-}$ signal measured by O K-NEXAFS and the activity of the $IrO_x$ anode in the oxygen evolution reaction (see Fig. 7c).

A comparison of $IrO_2$ and Pt electrodes in the OER seems to be very interesting. Pt electrodes which are worse anodes are characterized by the abundance of Ptδ+ states. Increasing the

voltage or the chemical potential induces the formation of Pt2- species, which are detrimental for the OER activity.

Since the relation between the abundance of the oxygen species $O^{I-}$ and the evolved oxygen was obtained by measurements in the gas phase there might be doubts, that these findings are relevant for the reaction in the liquid phase. A different approach is required in order to study the electronic structure of anode materials under oxygen evolution reaction conditions in the liquid phase.

**5. XPS investigation of electrochemically active solid-liquid interfaces**

The reaction cell which was developed for XPS measurements of electrodes in liquid electrolytes are based on electron transparent graphene. Kolmakov has shown, that XP spectra can be detected through graphene oxide membrane[18]. This idea was continued by Velasco who has demonstrated, that bilayers of graphene which are supported by silicon nitride grids with wholes of 1 μm enables the separation of liquid water on one side of the graphene and vacuum on the other side and the detection of XP spectra of an electrode surface under electrochemical reaction conditions[19]. It is well known, that graphene has a lot of energy related applications and in particular the functionalization with different materials results in a high activity in electrocatalytic reactions[20],[21]. Co anodes deposited on graphene show a considerable performance in the OER and[22] comparable or slightly higher than Pt[23] and Ir[24] functionalized C electrodes. The electrochemical functionalization of C with transition metals enables the control of the chemical properties and the morphology of the metal in order to increase its activity, selectivity and corrosion resistance[25]. Due to the lack of experimental methods suitable to deliver information on reactions occurring during electrochemical processes at the electrode-electrolyte interface on the atomic level the electronic structure of the Co particles and the interaction between the Co particle and the

graphene under OER reaction conditions remain unknown. Therefore an electrochemical cell was developed, which allows the estimation of the electronic structure of the electrochemically active interface between the graphene and the Co containing electrolyte. The liquid flow cell with the aqueous electrolyte circulating over the membrane (Fig.8), is prosecuted inside the main chamber of the endstation at the ISISS beamline of the synchrotron radiation facility BESSY. Hence a 4mM $CoSO_4$ solution was pumped through the cell and an under-potential deposition of the Co was performed at -1 V. The deposition consists of several processes like diffusion of electroactive species, desolvation, formation and incorporation of ad-atoms to the growing species. Anyway the electrochemical plating enables the control of the deposition rate and the oxidation state.

The Co deposit on the graphene was investigated with respect to the OER activity in a 10mM KOH solution. The CVs of the pristine graphene and the Co plated electrodes are plotted in Fig. 9. The CV of the electrodeposited Co is characterized by two oxidation peaks and one reduction peak[26]. Two anodic peaks at 0.6V(I) and 1.2V(II) are assigned to the oxidation of $Co^{2+}$ to $Co^{3+}$ and $Co^{3+}$ to $Co^{4+}$, respectively. The peak at 1.1 V(III) is assigned to the reduction of Co4+ to Co2+, with reversed potential , demonstrating that OER is preceded by Co oxidation. The electronic structure of the Co electrodeposited on the graphene was characterized by X-ray absorption spectroscopy (XAS) at the Co L-edges detected in the total electron yield (TEY) and in the total fluorescence yield (TFY) mode. The TEY spectra are assigned to the rock-slat CoO structure showing a peak at 777.4 eV, which is related to $Co^{2+}$[27] whereas the Co L-edge spectrum measured in the total fluorescence mode show an intense peak at 780.2 eV, which is characteristic for $Co^{3+}$ and therefore it can be assigned to $Co_3O_4$. Hence, the bonding of the Co to the graphene results in a reduction of the $Co^{3+}$ to $Co^{2+}$, which is linked to the replacement of O atoms by C in $Co_3O_4$ resulting in the formation of $Co(CO)_x$.

The Co2p XP spectrum measured during the electrodeposition of the Co is distinguished by the $2p_{1/2}$ and $2p_{3/2}$ spin orbit. The assignment of the peaks is provoking, since most of the Co species appear in a binding

energy range of 2.5 eV[28]. Obviously there exists some equivocality in peak assignment and quantification of such components indicated by similar binding energies[29]. Biesinger has suggested, that the deconvolution of 2p core level spectra of transition metal species can be performed by the application of a single-peak approach, due to multiplet splitting and satellite structure[30]. The interaction of C and Co can be compared to cobaltocene which was subject of an XPS study earlier[31]. The Co2p spectra show two main peaks at 783 eV and 798 eV due to spin orbit splitting in agreement with our measurements. The $Co2p_{3/2}$ core level spectrum was deconvoluted by two Gaussian-Lorentzian peaks at binding energies of 783.2 eV and 785.6 eV for peak A and peak B, respectively. In addition two shake-up satellites ($S_A$ and $S_B$) at 6 eV higher binding energies compared to the main peaks have to be considered. The intensity ratio of $Co2p_{3/2}$ /$Co2p_{1/2}$ was fixed to 2, in which the peak A at 783.2 eV has been assigned to $Co^{2+}$[32]. Therefore the peak A observed here at the same BE and which shows multiplet splitting and a satellite structure can be attributed to $Co^{2+}$ bound to C. The Co2p spectrum may contain in addition small amounts of $Co_xO_y(OH)_z$[33]. Furthermore the two peaks A and B can be assigned as well to Co bound to O like in carbonyl-like species as $Co(CO)_x$[34]. This assumption is confirmed by the comparison with pyrolyzed and porphyrin Co samples. In summary, the application of a new electrochemical in situ cell enabled the estimation of the electronic structure of Co electrodeposited on graphene. The interface is characterized by the formation of $Co(CO)_x$ species attended by the reduction of $Co^{3+}$ to $Co^{2+}$. Therefore, the increased electrocatalytic activity of Co/Graphene composites compared to graphene in the OER is likely related to the hybrid interface contacts, which control and promote the electron transfer reactions.

In the future OER reactions will be studied by this type of new electrochemical cells, but the investigation of OER is challenging since the released oxygen might burn the carbon particular at defects present in the graphene membrane with negative impact on the stability of the membrane. Therefore it is necessary to increase the stability of the membrane by passivating the top layer of the two layer graphene membrane or by using more that only two layers of graphene. In both cases the released photoelectrons have to pass a thicker membrane which will increase the scattering of the electrons in the membrane and therefore the intensity of the photoelectron spectrum will decrease significantly. Obviously it is preferable to get higher kinetic energy electrons released by the XPS process. Hence the application of higher photon energies is requested in order to obtain photoelectrons of higher kinetic energy. For that purpose the EMIL project was implemented by the Helmholtz Association and the Max-Planck Society was implemented.

The graphene was grown by CVD at 1050°C on a 25 µ thick Cu foil using $CH_4$. A polymer PMMA is spin coated onto the graphene and the copper foil is removed by $(NH_4)S_2O_8$. The graphene supported on the polymer was transferred onto the silicon nitride grid und the PMMA is dissolved acetone. It is very important that all wholes are covered completely by the graphene, since any leak will induce the formation of ice, due to the vacuum on the other side of the graphene, hence the silicon nitride grid will crack.

## 6. Outlook: The EMIL project @ BESSY

The Helmholtz Association and the Max-Planck-Society are implementing the EMIL (energy material in situ) Laboratory at the synchrotron radiation facility BESSY in Berlin. The main idea of the project is the implementation of two undulator beamlines. The soft X-ray beamline includes a plane grating monochromator and covers the soft X-ray range from 50

eV- 1.8 KeV. The tender X-ray beamline contains a double crystal monochromator and will provide photons in the range of 1.5 KeV- 8 KeV. The foci of the two beamlines will be located at the same position. This will enable photoelectron spectroscopy unter reaction conditions in the energy range for 50 eV- 8 KeV. The electron energy analyzed has near ambient pressure capabilities up to 7 KeV. The X-rays of the two undulators can be switched between beamlines delivering photons to two laboratories. The SISSY (XXX) lab is dedicated to the investigation of semiconductor interfaces prepared in the same laboratory and transferred under UHV into the analytic chamber, which enabled XPS, XES,…. studies. The CAT (catalysis) lab is designed for the investigation of heterogeneous reactions and electrochemical processes by Near Ambient Pressure Photoelectron Spectroscopy. The analyzer can be operated with different sample environment modules. One advantage of the modular concept is the fact, that the heterogeneous catalytic reaction or the electrochemical process can be optimized already before the measurements performed at the EMIL beamlines. The CAT laboratory provides the related infrastructure like central and local gas supply gas analytics, electrochemical devices, etc.

The tender X-ray photons will release photoelectrons with kinetic energies in the range of a few tens of eV up to 8 KeV. In particular the higher kinetic energy electrons will have a higher electron mean free path of a few 10 nm in carbon, which enables the electrons to even pass a few layers of graphene of similar materials. This fact is of very high relevance for the in situ investigation of the oxygen evolution reaction in liquid water. The strong interaction of the released oxygen with any defects in the graphene layers requires the application of more than just two graphene layers to form a stable membrane, which resists a pressure difference of 1 bar on one hand, but providing still sufficient electron transparency for the photoelectrons created by the X-ray photoelectron process.

The tuneability of the synchrotron radiation enables depth profiling measurements perpendicular to the electrode/electrolyte interface. This will offer the possibility to optimize the detection of electrons released from the electrolyte/electrode interface.

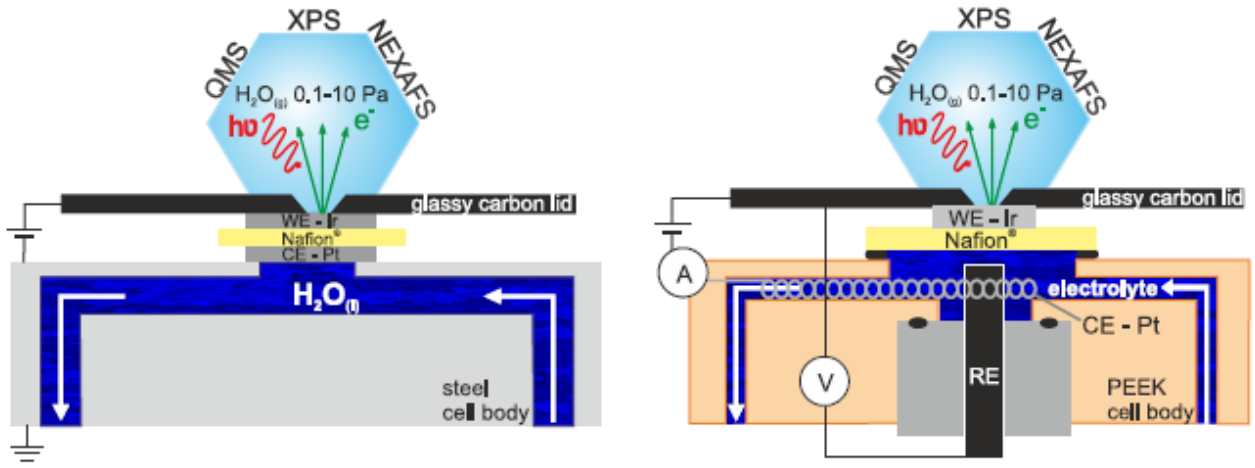


**Fig. 1** (left) Two-electrode in situ cell with sputtered Ir working and Pt counter electrode. (right) Three-electrode in situ cell with sputtered Ir working, Pt wire counter, and ag/AgCl reference electrode. In both cells, water supplied from the rear diffuses through the desiccation cracks of the sputtered electrodes and the PEM and delivers the reactant molecules to the reaction chamber. While XPS and NEXAFS are measured, the gas composition is monitored by an on-line quadrupole mass spectrometer (QMS). Through the connection to an external potentiostat, OER relevant potentials can be applied to the working electrode [adapted from pfeifer Chemical science].

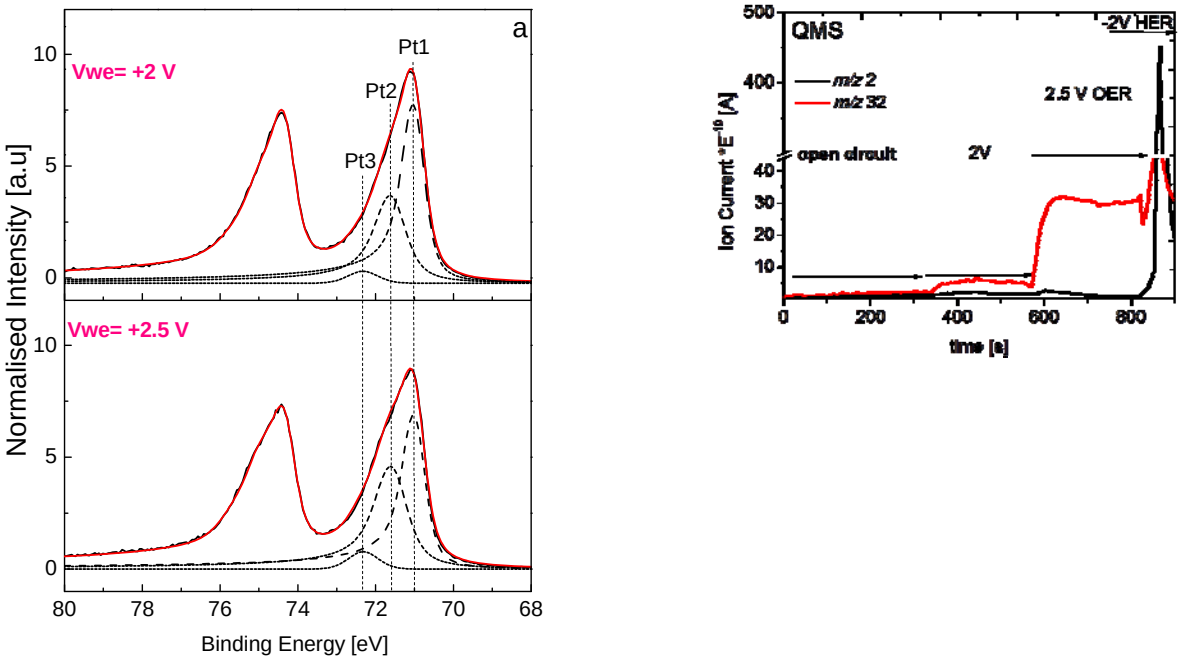


Fig. 2: a) Pt4f spectra measured at 600 eV kinetic energy of the electrons. The information depth is approximately 2.5 nm. The components Pt1,Pt2 and Pt3 represent the metallic Pt, the adsorbed oxygen species on Pt and $Pt^{2+}$ respectively. b) [adapted from 5] QMS signals during the XPS measurements

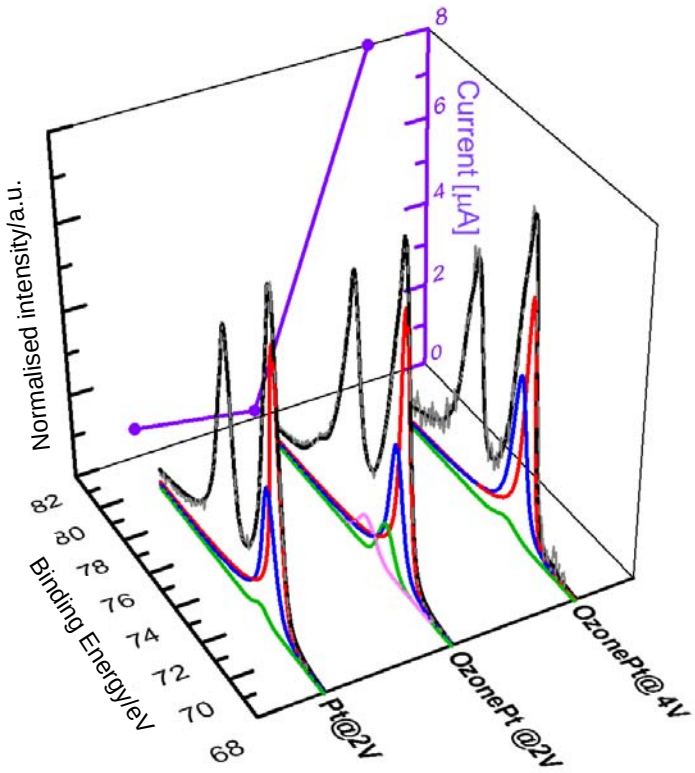


Fig. 3. Pt/Nafion/Pt versus Ag wire reference electrode: Pt4f spectra (KE=150 eV) during constant anodic polarization and the corresponding measured current for the sputtered Pt film WE at 2V, and at 2V and 4V after pretreatment in 1 bar $O_3$; the order indicates chronological sequences of the experiments.

a)

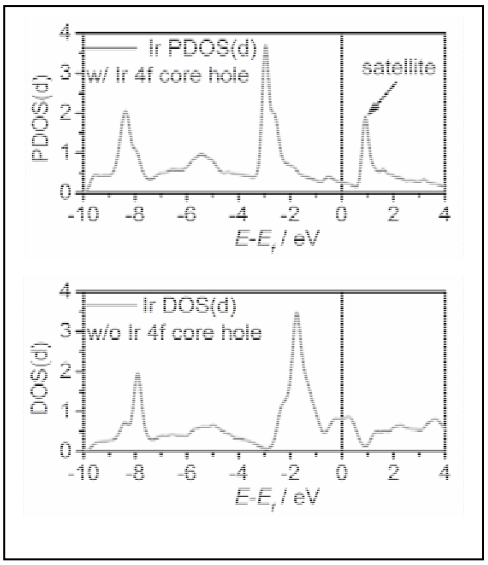


b)

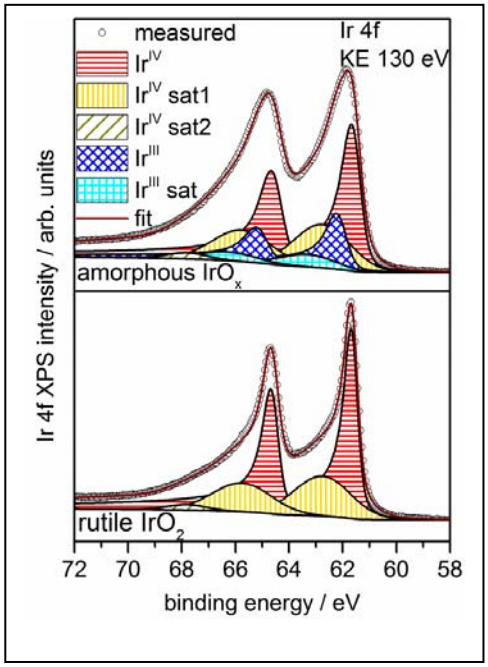


Fig.4: a) Calculated PDOS (d) of rutile $IrO_2$ in the presence of a 4f core hole (top) and without a core hole (bottom). b) Ir4f spectra of amorphous IrOx (top spectrum) and Ir4f spectrum of rutile like $IrO_2$ (bottom spectrum)

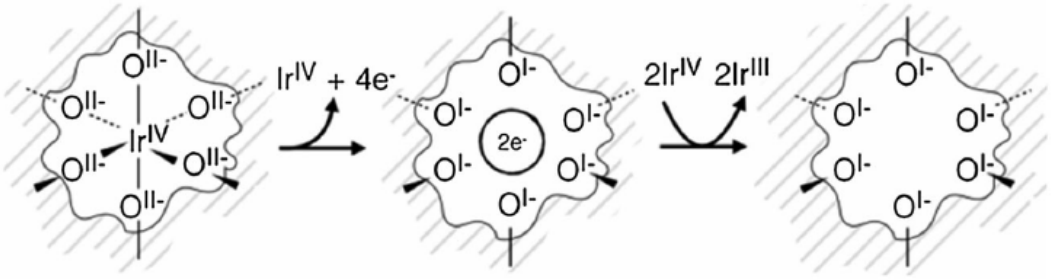


Figure 5: Scheme of transformations in the anionic and cationic framework upon the introduction of an Ir vacancy. Reproduced from SIA

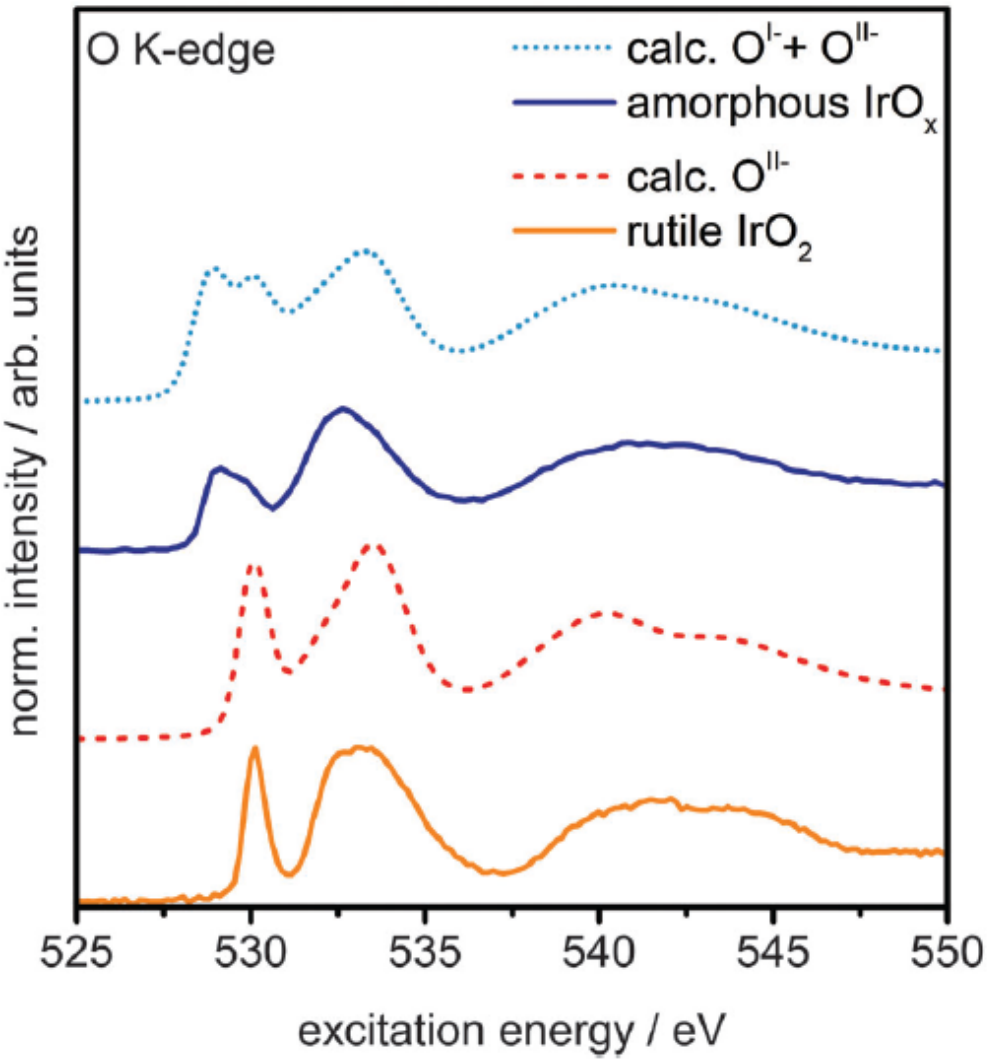


Fig.6: Measured O K-edge spectra of rutile $IrO_2$ and amorphous $IrO_x$ and calculated O K-edges of OII- and a linear combination of 60% $O^{II-}$ and 40% $O^{I-}$ species. Reproduced from PCCP

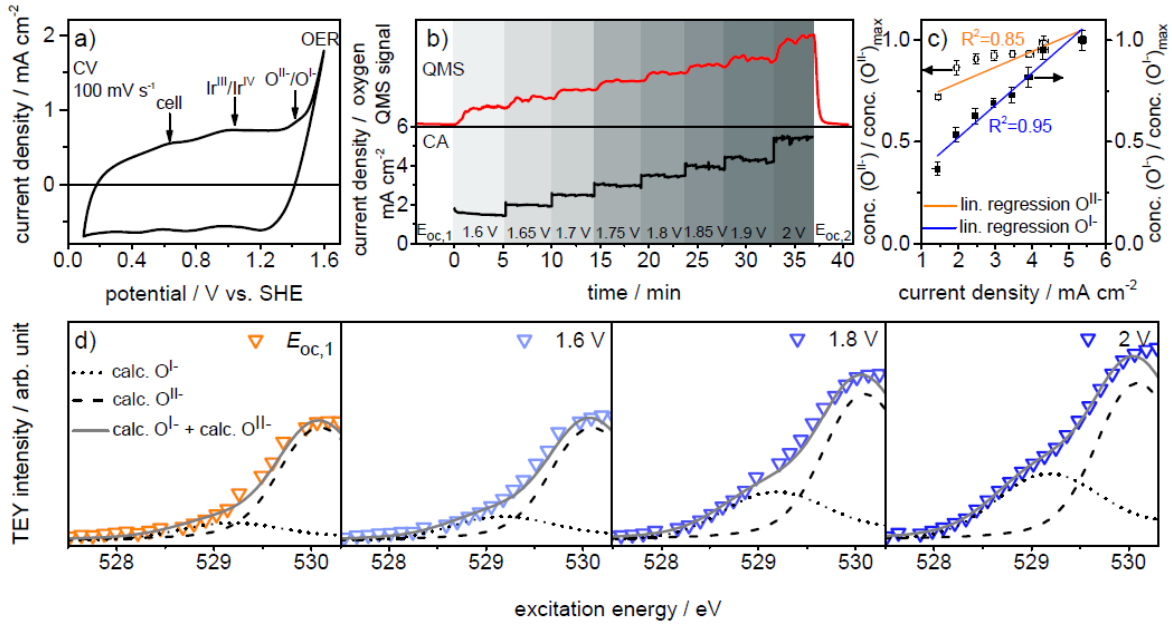


Figure 7: a) Cyclic voltammogram, b) chronoamperometry (bottom) and oxygen QMS signal (top), c) normalized OI- and OII-concentration over current density, and d) zoomed and fitted low excitation energy regions of O K-edge recorded in the three-electrode cell (indicated potentials vs. SHE, ring current: 60 mA, p=0.3Pa, 0.1 M $H_2SO_4$) (reproduced from chem sci in situ)

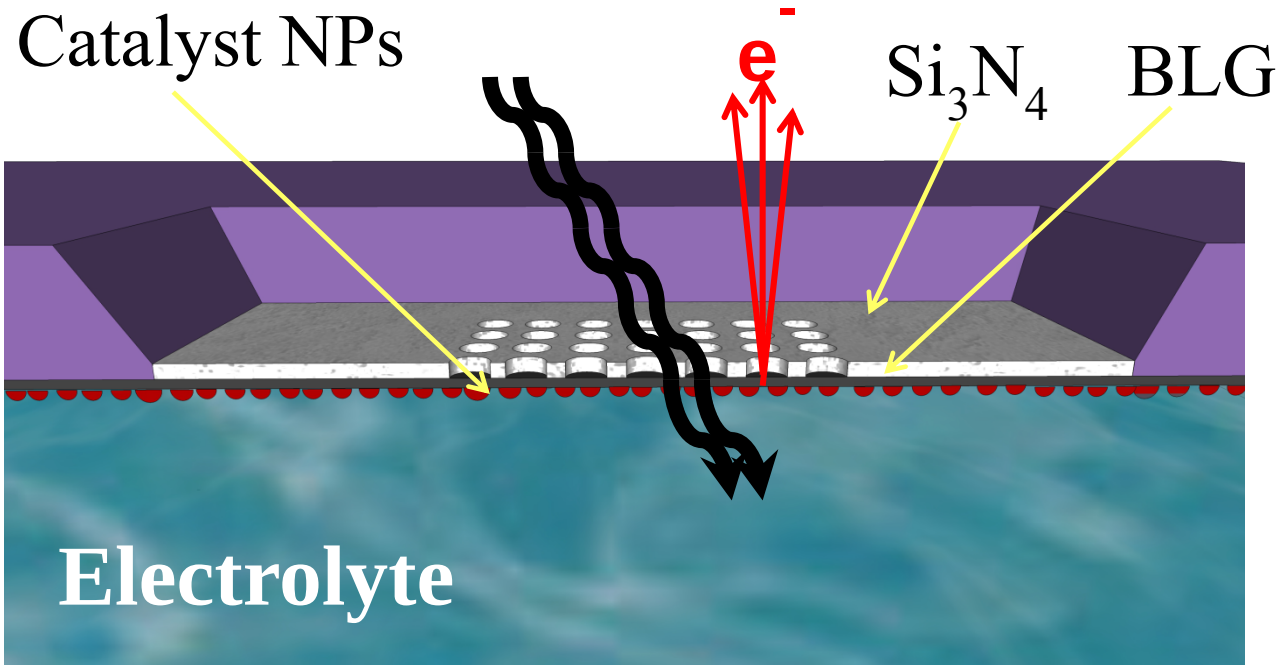


Figure 8: Schematic cross section of the liquid flow cell

## References


1 M. Beaudin, H. Zareipour, A. Schellenberglabe, W. Rosehart, Energy Sustainable Dev. 2010, 14, 302.

2 R. Schlögl, ChemSusChem 2010, 3, 209.

3 A. Ursua, L. M. Gandia, P. Sanchis, Proc. IEEE2012, 100, 410.

4 F. Schüth, Energy storage strategies, in R. Schlögl, Editor, Chemical Energy Storage, De Gruyter, Berlin, 2012, pp. 35-47.

5 R. Arrigo, M. Hävecker, M. E. Schuster, C. Ranjan, E. Stotz, A. Knop-Gericke, R. Schlögl, Angew. Chem. Int. Ed. 2013, 52, 11660-11664

6 A. K. N. Reddy, M. A. Genshaw, J. O'M Bockris, J. Chem. Phys. 1968, 48, 671

7 Z. Zhu, F. Tao, F. Zheng, R. Chang, Y. Li, L. Heinke, Z. Liu, M. Salmeron, G. A. Somorjai, Nano Lett.. 2012, 12, 1491-1497

8 D. J. Miller, H. Öberg, S. Kaya, H. Sanchez Casalongue, D. Friebel, T. Anniyev, H. Ogasawara, L. G. M. Petterson, A. Nilsson, Phys. Rev. Lett. 2011, 107, 1955021-1955025

9 A. E. Bolzan, A. J. Arvia, J. Electroanal. Chem. 1992, 341, 93-109.

10 M. Peukert, H. ibach, Surf. Sci. 1984, 136, 319-326.

11 A. Damjanovic, V. I. Birss, D. S. Boudreaux, J. Electrochem. Soc. 1991, 138, 2549-2555.

12 G. K. Wertheim, S. Hüfner, Phys. Rev. Lett. 1975, 35,53

13 G. K. Wertheim, H. J. Guggenheim, Pyhs. Rev. B 1980, 22, 4680

14 V. Pfeifer, T. E. Jones, J. J. Velasco-Vélez, C. Massué, M. T. Greiner, R. Arrigo, D. Teschner, F. Girgsdies, M. Scherzer, J. Allan, M. Hashagen, G. Weinberg, S. Piccinin, M. Hävecker, A. Knop-Gericke, R. Schlögl PCCP 2016, 18, 2292-2296

15 V. Pfeifer, T. E. Jones, J. J. Velasco-Veléz, C. Massué, R. Arrigo, D. Teschner, F. Girgsdies, M. Scherzer, M. T. Greiner, L. Allan, M. Hashagen, G. Weinberg, S. Piccinin, M. Hävecker, A. Knop-Gericke, R. Schlögl, Surf. Interface Anal. 2016, 48, 261-273

16 V. Pfeifer, T. E. Jones, S. Wrabetz, C. Massué, J. J. Velasco-Vélez, R. Arrigo, M. Scherzer, S. Piccinin, M. Hävecker, A. Knop-Gericke, R. Schlögl, Chem. Sci. 2016, 7, 6791

17 V. Pfeifer, T. E. Jones, J. J. Velasco-Vélez, R. Arrigo, S. Piccinin, M. Hävecker, A. Knop-Gericke, R. Schlögl, Chem. Sci, submitted

18 A. Kolmakov, D. A. Dikin, L. J. Cote, J. Huang, M. K. Abyaneh, M. Amati, L. Gregoratti, S. Günther and M. Kiskinova, Nat. Tech. 2011, 6, 651-657

19 J. J. Velasco-Vélez, V. Pfeifer, M. Hävecker, R. S. Weatherup, R. Arrigo, C.-H. Chuang, E. Stotz, G. Weinberg, M. Salmeron, R. Schlögl, and A. Knop-Gericke, Angew. Chem. Int. Ed. 2015, 54, 14554-14558

20 a) S. Bai, X. Shen, RSC Adv. 2012, 2, 64-98; b) B. F. Machado, P. Serp, Catal. Sci. Technol. 2012, 2, 54-75; c) S. Bose, T. Kuila, A. K. Mishra, R. Rajasekar, N. H. Kim, J. H. Lee, J. Mater. Chem. 2012, 22, 767-784

21 a) Z. S. Wu, G. Zhou, L. C. Yin, W. Ren, F. Li, H. M. Cheng, Nano Energy 2012, 1, 107-131; b) Y. Liang, Y. Li, H. Wang, J. Zhou, J. Wang, T. Regier, H. Dai, Nat. Mater. 2011, 10, 780-786

22 S. Mao, Z. Wen, T. Huang, Y. Hou, J. Cheng, Energy Environ. Sci. 2014, 7, 609-616

23 J. Wang, J. Zhou, Y. Hu, T. Regier, Energy Environ. Sci. 2013, 6, 926-934

24 L. Wu, C. H. Wu, H. Zhu, A. Mendoza-Garcia, B. shen, J. Guo, S. Sun, J. Am. Chem. Soc. 2015, 137, 7071-7074

25 B. Bozzini, P. Bocchetta, A. Gionancelle, C. Mele, M. Kiskinova, Acta Chim. Slov. 2014, 61, 263-271.

26 J. Ismail, M. F. Ahmed, P. V. Kamath, , J. Power Sources 1991, 36, 507-516

27 Q. He, Q. Li, S. Khene, X. Ren, F. E. Lopez-Suarez, D. Lozano-Castello, A. Bueno-Lopez, G. Wu, J. Phys. Chem. C 2013, 117, 8697-8707

28 J. J. Pietron, J. C. Biffinger, S. B. Qadri, D. R. Rolison, J. Mater. Chem. 2011, 21, 7668-7677.

29 K. Artyushkova, S. Levendosky, J. Fulghum, P. Aanassov, Top. Catal. 2007, 46, 263-275.

30 M. C. Biesinger, B. P. Payna, A. P. Grosvenor, L. W. M. Lau, A. R. Gerson, R. S. C. Smart, Appl. Surf. Sci. 2011, 257, 2717-2730.

31 C. K. Chan, A. Khan, Q. Zhang, S. Barlow, S. R. Marder, Appl. Phys. 2007, 102, 014906.

32 a) X. Xiang, L. Zhang, H. I. Hima, F. Li, D. G. Evans, Appl. Clay Sci. 2009, 42, 405-409; b) V. Musat, E. Fortunato, A. M. B. Do Rego, r. Monteiro, thin Solid Films 2008, 516, 1499-1502; c) R. S. Da Cruz, A. J. S. Mascarenhas, H. M. C. Andrade, Appl. Catal. B 1998, 18, 223-231.

33 a) S. Cobo et al., Nat. Mater. 2012, 11, 802-807; b) R. Xu, H. C. Zeng, Chem. Mater 2003, 15, 2040-2048

34 a) K. Artyushkova, S. Pylypenko, T. S. Olson, J. E. Fulghum, P. Atanasov, Langmuir 2008, 24, 9082-9088; b) S. Pylypenko, S. Mukherjee, T. S. Olson, P. Atanassov, Electrochim. Acta 2008, 53, 7875-7883; c) T. S. Olson, S. Pylypenko, P. Atanassov, K. Yamada, H. Tanaka, J. Phys. Chem. C 2010, 114, 5049-5059